OPO OPHTHALMIC & PHYSIOLOGICAL OPTICS
THE JOURNAL OF THE COLLEGE OF OPTOMETRISTS

Ophthalmic & Physiological Optics ISSN 0275-5408

Calculation of the geometrical point-spread function from wavefront aberrations

Larry N Thibos

School of Optometry, Indiana University, Bloomington, USA

Citation information: Thibos LN. Calculation of the geometrical point-spread function from wavefront aberrations. *Ophthalmic Physiol Opt* 2019; 39: 232–244. https://doi.org/10.1111/opo.12619

Keywords: aberrations, astigmatism, optics

Correspondence: Larry N Thibos
E-mail address: thibos@indiana.edu

Received: 17 January 2019; Accepted: 10 April 2019

Author contributions: The author certifies that he has participated sufficiently in the work to take public responsibility for the content, including participation in the concept, design, analysis and writing or revision of the manuscript.

Abstract

Purpose: This report uses the principles of geometrical optics to compute the optical point-spread function (PSF) from the wavefront error function.
Method: Step 1 uses Prentice's rule to determine the spatial form of the PSF established by tracing a field of rays from the eye's exit pupil to the retina. Ray vergence is related to the slope of the wavefront error function, which enables the mapping of light rays to produce a retinal 'spot diagram'. Step 2 completes the PSF by assigning an irradiance value to each ray in the spot diagram.
Results and Conclusions: Spot irradiance is inversely proportional to the Gaussian curvature (i.e. the product of principal curvatures) of each local region of wavefront error surface centered on the corresponding ray. The Gaussian curvature, in turn, may be computed as the determinant of the vergence error matrix associated with each point on the wavefront error surface. Elements of the vergence error matrix consist of sums and differences of the local power vector components M, J_0 and J_{45}. This method is shown to be equivalent to published derivations of the geometric PSF using the Jacobian of the ray mapping function and equivalent also to the Hessian of the wavefront error function. Examples are presented for the familiar cases of spherical and astigmatic blur as well as for higher order aberrations and the formation of caustics in the retinal image.

Introduction

The optical point-spread function (PSF) is a fundamental measure of the imaging quality of an eye that can be reduced to a variety of single-number metrics of retinal image quality useful for determining the eye's refractive error, state of accommodation, optical limits to visual performance, and optical performance of contact lenses, inter-ocular lenses, and corneal refractive surgery.[1] Calculation of the eye's PSF from wavefront aberration measurements is typically based on the principles of physical optics, which include the effects of diffraction and interference of light.[2] On the other hand, most practical problems in clinical and visual optics are solved using the simpler methods of geometrical optics. It seems likely, therefore, that improved understanding of the optical basis for computing the geometric PSF will benefit many aspects of clinical practice and applied vision research.

Geometric optics uses rays to describe the propagation of light through optical systems to form images. The example in *Figure 1* illustrates rays of light from a distant point source being refracted by an ideal lens of power F, which causes all the rays to intersect at a common focal point P located at an axial distance $d = 1/F$ from the lens. According to Prentice's rule,[3] refraction of an isolated ray displaced by amount r from the optical axis causes the ray to deviate by angle $\Delta = rF$. Since the ray is parallel to the optical axis in this example, Δ is also the angle between the refracted ray and the optical axis. Assuming small angles, $\Delta = \tan(\Delta) = r/d$, and noting that vergence V of the ray emerging from point Q in *Figure 1* is defined by the inverse of the distance d, it follows that the vergence V of the emerging ray is $1/d = \Delta/r$.

We conceive of wave propagation as motion in a direction perpendicular to the wave and thus in the direction indicated by rays drawn normal to the wavefront surface. Thus ray vergence as defined above may also be interpreted as wavefront vergence at the point Q of intersection of wavefront and ray. A line tangent to the wavefront at Q is

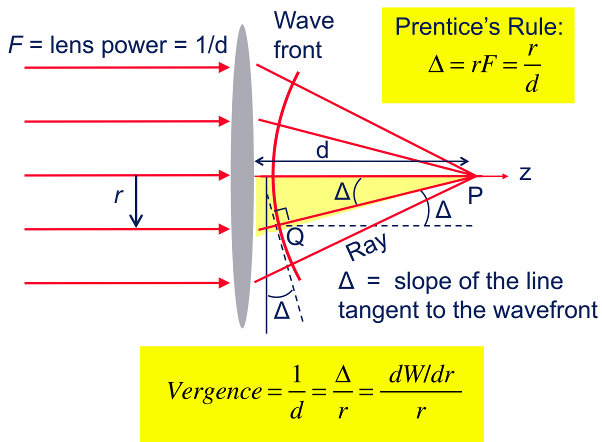

Figure 1. Geometry of ray deflection by a rotationally symmetric lens.

also perpendicular to the ray emerging from Q and therefore, according to the geometry of the diagram, Δ is also the angle between this tangent line and a reference plane (e.g. the exit pupil) perpendicular to the optical axis. For this reason Δ can be interpreted as the slope of the wavefront at Q, which implies that Prentice's rule is also a statement about wavefront slope. That statement is made explicit by representing the wavefront's shape by a mathematical function $z = W(r)$. The radial slope of this function at the point $z = W(r)$ is denoted by the spatial derivative $\mathrm{d}W/\mathrm{d}r$ which, according to *Figure 1*, is equal to the angle Δ. Thus, when written in terms of wavefront slope, Prentice's rule equates ray vergence Δ/r with wavefront vergence $(\mathrm{d}W/\mathrm{d}r)/r$,

$$V = \frac{\Delta}{r} = \frac{\mathrm{d}W/\mathrm{d}r}{r}. \qquad (1)$$

Anticipating potential confusion of terminology, we note that a parabolic wavefront specified by the function $W = ar^2$ is a surface of constant vergence (=$2a$) according to *Equation* 1. Thus, according to Prentice's rule, a paraboloid of revolution is the ideal wavefront that focuses to a single image point. This is not strictly true, however, because *Equation* 1 assumes that the radial location of point Q on the curved wavefront is identical to the radial displacement of the ray in the reference plane of the exit pupil. This is a reasonable approximation provided wavefront slope Δ is small, but it restricts the domain of Prentice's rule (and its further development in this report) to the paraxial domain. In fact, the ideal wavefront has spherical shape but it is common language to refer to its parabolic approximation as a spherical wavefront. We also note that wavefront curvature in the paraxial domain is given approximately by the second derivative of the wavefront, which for the parabolic wavefront $W = ar^2$ also equals $2a$, the wavefront vergence according to *Equation* 1. Geometrically, this equality implies the local centre of curvature for the portion of wavefront near point Q in *Figure 1* lies at point P, which is only approximately true for a paraboloid (but is exactly true for a sphere). Nevertheless, this approximate equality explains why the terms vergence and curvature are often used synonymously when describing wavefronts even though they are different geometrical concepts.[4,5]

Equation 1 is the starting point for developing a general formula for computing the PSF using geometrical optics. This development is presented below in three stages, beginning with the simplest case of spherical wavefronts, generalising to the slightly more complicated case of spherocylindrical wavefronts, and finishing with the general case of wavefronts containing higher order aberrations. At each successive stage the mathematics will require some elaboration, but the emphasis is on optical explanations based on familiar concepts such as wavefront curvature, power vectors,[6] vergence error matrices,[7,8] and Gaussian curvature. The overarching goal is to make the development clinically accessible by appeal to basic optical principals, keeping the mathematical formulas as simple as possible. The main result is an explicit formula for the geometric PSF in terms of wavefront vergence. Several equivalent formulas for the PSF are provided to foster a deeper understanding achieved by approaching the topic from multiple directions. One application of these formulas is to explore the formation of optical caustics in the retinal plane commonly known as visual starbursts.[9,10]

Methods and results

Blur disks for spherical defocus

Light rays in *Figure 1* converge to a single image point P but if a screen is placed at some other z-axis location, then the blurred image formed on the screen will be a uniformly illuminated, circular disk of light. This disk of light is the geometric PSF for an optically perfect, but defocused, eye. Our initial goal is to determine the diameter and irradiance of this blur disk. The answer is already well known[11] so the aim here is to illustrate an approach that can be generalised to handle astigmatism and higher-order aberrations.

The geometry of the problem is shown in *Figure 2*. Since spherical wavefronts are rotationally symmetric, it is sufficient to consider a single cross section of the wavefront (centred on point G) and the reference sphere (centred on point R). The reference sphere represents an ideal spherical wavefront for which all rays intersect at the point R on the image screen. One such reference ray is the line AR, which is perpendicular to the reference sphere at point A. The defocused marginal ray of light is perpendicular to the wavefront of light at point B and intersects the image screen

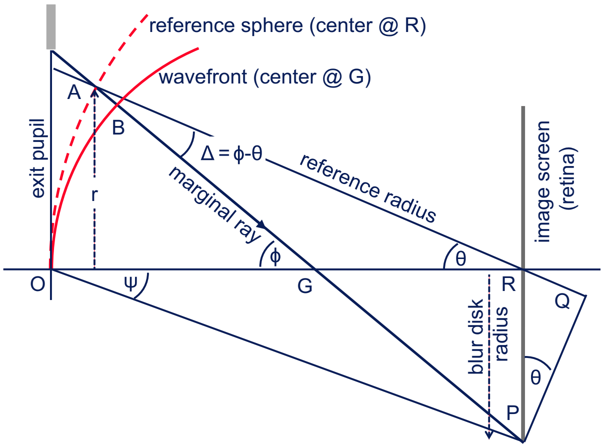

Figure 2. Ray aberrations determine the mapping of pupil coordinates to corresponding visual coordinates of a ray's intersection with the image screen.

at point P. Thus the blur disk radius is equal to the length of line RP. We wish to express the blur disk radius as a visual angle ψ subtended by the line RP at the centre of the exit pupil.

With reference to *Figure 2* and *Equation* 1, the angle θ between the reference radius AR and the optical axis OR is also the slope of the reference sphere at point A. Similarly, the angle ϕ between the marginal ray and the optical axis is also the slope of the wavefront near point A (in this context we are neglecting the very small separation between points A and B). From the geometry of right triangles we infer that the angle Δ between the marginal and reference rays, called the angular ray aberration, equals $\phi - \theta$ and thus is equal to the difference in slopes of the wavefront and reference sphere at point A. From right triangle AQP we know that $\tan \Delta = PQ/AQ$. For small amounts of defocus the distance QR is negligible compared to AR, which justifies approximating AQ by the reference radius AR = OR. Thus we have established one approximate relationship,

$$\tan \Delta \cong \frac{PQ}{OR}. \qquad (2)$$

From right triangle ORP we know that $\tan \psi = PR/OR$. If the reference angle θ is small, PQ is approximately equal to PR, which gives a second approximate relationship,

$$\tan \psi \cong \frac{PQ}{OR}. \qquad (3)$$

Taken together, *Equations* 2 *and* 3 imply that ψ, the angular radius of the blur disk is approximately equal to Δ, the angular ray aberration. This result can be expressed in terms of pupil radius and dioptres of defocus by applying Prentice's rule embodied in *Equation* 1. The vergence of the marginal ray of light is ϕ/r whereas the vergence of the reference ray is θ/r. This vergence difference $E = (\phi - \theta)/r = \Delta/r$, where E is the focusing error in dioptres. This result confirms Smith's approximate formula $\psi \cong \Delta = rE$ for the angular radius ψ (in radians) of the blur circle expressed as the product of pupil radius r (in meters) with defocus E (in dioptres).[11] One advantage of expressing the size of the blur circle as a visual angle is that the value does not depend on the distance from exit pupil to image screen. Thus ψ applies equally well to the retinal image of an external point source and for the areal image formed outside the eye of a point source on the retina.

The preceding analysis for a point A on the pupil margin may be applied to any point on the wavefront. Doing so leads to the key result that the location of a ray's intersection with the retinal plane, expressed as a visual angle ψ subtended at the pupil centre, is approximately equal to the ray aberration $(\phi - \theta)$. From the geometry of *Figure 1*, the angles ϕ and θ are equal to the slopes (i.e. first derivatives) of the wavefront and the reference sphere, respectively. Since differentiation is a linear operation, the difference of derivatives is equal to the derivative of the differences and therefore the visual angle ψ is equal to the slope of the wavefront error (WFE) function computed by subtracting the reference sphere from the wavefront. This equality between visual angle and WFE slope suggests further development be based on the WFE function (rather than the wavefront itself) as a way to simplify the analysis and make generalised conclusions without concern for the underlying wavefront of light and the reference sphere associated with the physical layout of the optical system.

To complete the description of the geometrical PSF for spherical defocus we also need to specify the irradiance at each point inside the blur disk. An intuitive way to determine the answer is to consider ray density in the image plane that results from a set of uniformly spaced rays in the pupil plane. Applying Prentice's rule to each ray inside the pupil, just as we did above for the marginal ray, will give the angular location of each ray's intersection with the retinal image plane. The answer for spherical defocus is easily deduced because vergence of a spherical wavefront is the same at every point on the wavefront. Similarly, the vergence of a reference ray is independent of pupil location and therefore the vergence error is the same for all rays passing through the pupil. As shown above, the angular displacement of the ray's intersection with the retina (e.g. point P in *Figure 2*) is equal to vergence error times pupil location r. Since vergence error is constant, retinal location of rays will be proportional to their pupil location. In other words, uniformly spaced rays in the pupil will be uniformly spaced on the retina. Thus ray density is uniform, and so is the geometrical PSF. For a given amount of light flux entering the eye, the uniform irradiance of the blur disk will be inversely proportional to the area of the blur circle. The larger the blur disk, the lower the irradiance.

Blur disks for defocus with astigmatism

Astigmatism disrupts the rotational symmetry that simplified the preceding derivation of the geometrical PSF for pure defocus. When astigmatism is present, *Figures 1 and 2* are valid only for light rays in the principal meridians (i.e. meridians parallel to and orthogonal to the axis of the astigmatism). For rays in other meridians the diagram is misleading because after refraction the rays no longer lie in the plane of the diagram and therefore do not intersect the optical axis (i.e. they are skew rays). Handling skew rays will require an extension of the mathematical treatment given above, but before taking that step we can estimate the size of the blur disk on the retina using Smith's formula $\Delta = rE$. This formula remains valid if we confine attention to the principal meridians of the astigmatic component of the WFE where the rays are not skew. To simplify the exposition initially, we assume the principal meridians correspond to the x- and y- axes of a Cartesian reference frame centred on the pupil as shown in *Figure 3*.

To illustrate the general case of blurred images in both principal meridians, *Figure 3* depicts a vertical sheet of rays from a point source focusing in front of the retina and a horizontal sheet of rays focusing behind the retina. The dioptric focusing error E_v for the vertical meridian is larger than the focusing error E_h for the horizontal meridian in this example, so (according to *Figure 1*) the blur disk on the retina will have a greater extent vertically than horizontally. Applying Smith's formula to the principal meridians, the major and minor angular radii of the blur disk will be

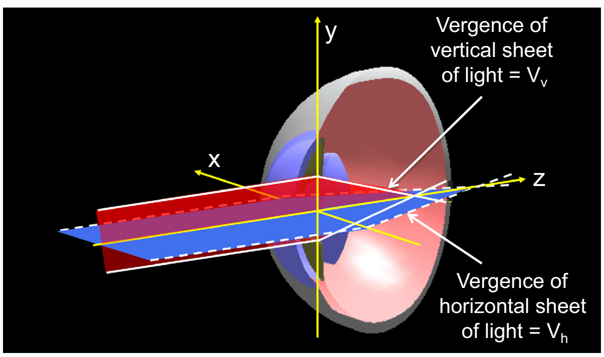

Figure 3. Refraction of sheets of rays in the principal meridians of an eye with sphero-cylindrical aberrations. In this example, the vertical sheet focuses anterior to the retina and the horizontal sheet focuses posterior to the retina. The result is a uniformly irradiated blur disk with elliptical perimeter.

$\Delta_v = rE_v$ and $\Delta_h = rE_h$. It will be shown below that the perimeter of the blur disk is an ellipse, which collapses to a circle (the 'circle of least confusion') when the retina lies at the dioptric midpoint of Sturm's interval.[12] It will also be shown that the irradiance of the blur ellipse is uniform, just as for pure defocus.

Visualising skew rays, their vergence, and where they intersect the retinal plane requires three-dimensional diagrams that are difficult to render on paper. This difficulty introduced by astigmatism is further compounded by higher order aberrations that, in general, cause all rays to be skew. To help envision the propagation of wavefronts from exit pupil to retina, dynamic simulations are described in the Appendix. The rest of this report, however, is concerned not with the wavefront *per se*, but with the WFE function, which is the difference between the wavefront and the reference sphere. Nevertheless, some necessary concepts can be grasped by envisioning the WFE function as a propagating wavefront surface as illustrated in *Figure 4*. This example illustrates the type of WFE expected for an astigmatic system with vertical and horizontal principal meridians (e.g. *Figure 3*). By comparison, a perfect optical system would have WFE = 0 everywhere in the exit pupil, which would be indicated by a plane wave focusing at infinity. Areas of the WFE surface that are converging indicate the wavefront of light is locally more curved than the reference sphere and therefore will be blurred in the image plane. Conversely, areas of the WFE surface that are diverging indicate the wavefront of light is locally less curved than the reference sphere, which again produces blur in the image. Thus the magnitude of curvature of the WFE surface at some location indicates the degree to which light from that location will be blurred in the image plane.

An appreciation for WFE slope in three dimensions can be gathered by considering a ray perpendicular to the WFE surface at some point A in *Figure 4*. The three-dimensional counterpart to the dashed tangent line of *Figure 1* is a plane tangent to the WFE surface at A that is also perpendicular to the ray. The tangent plane has a degree of tip and tilt that corresponds to wavefront slope in the x- and y- directions. To see why, intersect the tangent plane with a horizontal plane (y = constant) through A to produce the red line, the slope of which in the horizontal plane is the partial derivative $\partial W/\partial x$. Similarly, intersecting the tangent plane with a vertical plane (x = constant) through A produces the blue line, the slope of which in the vertical plane is the partial derivative $\partial W/\partial y$. Following the analysis of *Figure 2* given above, the horizontal and vertical components of slope (called the gradient of the WFE function, denoted ∇W) are approximately equal to the horizontal and vertical components (α, β) of the visual angle of the point of

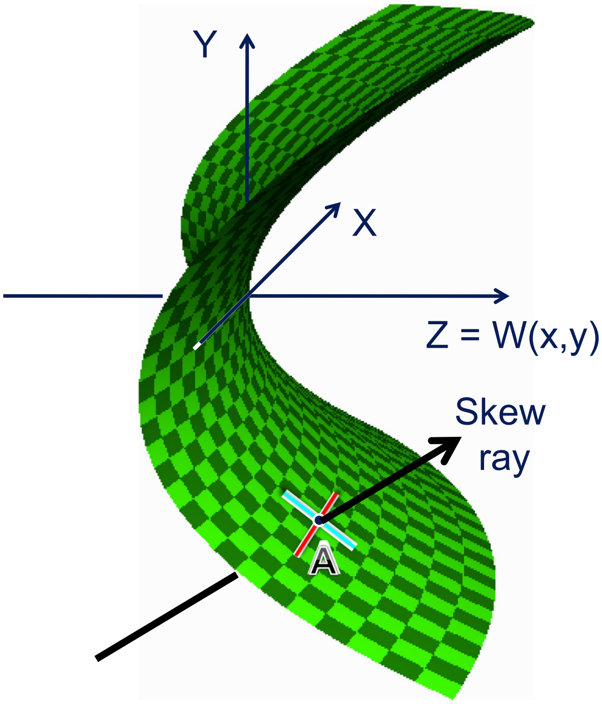

Figure 4. Geometry for specifying tip and tilt of a plane tangent to the wavefront error surface at point A. Intersection of the tangent plane with horizontal and vertical planes through A are indicated by the red and blue lines, respectively, for which the slopes are equal to the partial derivatives $\partial W/\partial x$ and $\partial W/\partial y$.

intersection in the retinal image plane made by the ray from point A,

$$\nabla W = \mathrm{grad}(W(x,y)) = \left[\frac{\partial W}{\partial x}, \frac{\partial W}{\partial y}\right] \cong [\alpha, \beta]. \quad (4)$$

In summary, given an algebraic formula $W(x,y)$ for the WFE function, the x- and y- slopes can be computed analytically or numerically as the partial derivatives $\partial W/\partial x$ and $\partial W/\partial y$. These slopes are the gradient of $W(x,y)$ and are approximately equal to the visual coordinates of the ray's intersection with the retinal plane. Decomposing WFE slope into a pair of orthogonal components this way simplifies the calculation of ray (and wavefront) propagation to the image plane by separately computing the horizontal and vertical components of the ray.[13] Similarly, as will be shown below, decomposing wavefront vergence into its horizontal and vertical components simplifies the calculation of the geometrical PSF for astigmatic systems and when higher-order aberrations are present.

To demonstrate the approach outlined above, consider the problem of finding the shape of the blur disk by an astigmatic imaging system. In the absence of higher-order aberrations, the WFE function $W(x,y)$ can be described by the weighted sum of second-order Zernike polynomials.[14] Although these polynomials are conventionally expressed in terms of normalised pupil coordinates, here it is more convenient to use physical coordinates thereby showing pupil radius explicitly.

$$\begin{aligned} W(x,y) &= C_2^0 Z_2^0 + C_2^2 Z_2^2 + C_2^{-2} Z_2^{-2} \\ &= C_2^0 \sqrt{3}\left(2(x/R)^2 + 2(y/R)^2 - 1\right) \\ &\quad + C_2^2 \sqrt{6}\left((x/R)^2 - (y/R)^2\right) \\ &\quad + C_2^{-2} 2\sqrt{6}\left((x/R)(y/R)\right). \end{aligned} \quad (5)$$

In this equation x, y are pupil coordinates in physical units, R is pupil radius, C_2^0, C_2^2, C_2^{-2} are the Zernike coefficients, and Z_2^0, Z_2^2, Z_2^{-2} are the Zernike polynomials for defocus, astigmatism with principal curvatures in the horizontal (0°) and vertical (90°) meridians, and astigmatism with principal curvatures in the obliquely oriented 45° and 135° meridians, respectively. The horizontal and vertical slopes of the wavefront at each (x,y) pupil location are determined by computing the partial derivatives of $W(x,y)$,

$$\begin{aligned} \frac{\partial W(x,y)}{\partial x} &= C_2^0 4\sqrt{3}x/R^2 \\ &\quad + C_2^2 2\sqrt{6}x/R^2 + C_2^{-2} 2\sqrt{6}y/R^2, \end{aligned} \quad (6)$$

$$\begin{aligned} \frac{\partial W(x,y)}{\partial y} &= C_2^0 4\sqrt{3}y/R^2 \\ &\quad - C_2^2 2\sqrt{6}y/R^2 + C_2^{-2} 2\sqrt{6}x/R^2, \end{aligned} \quad (7)$$

If pupil coordinates and radius are specified in mm and Zernike coefficients are in microns, then *Equations* 6 *and* 7 for the WFE gradient can be expressed in clinical dioptric units associated with power vector components $M = C_2^0 4\sqrt{3}/R^2$ for defocus, $J_0 = C_2^2 2\sqrt{6}/R^2$ for 0°/90° astigmatism, and $J_{45} = C_2^{-2} 2\sqrt{6}/R^2$ for 45°/135° astigmatism (see *equation* 1 of reference 1). According to *Equation* 4, the results are approximately equal to the visual angles α, β

$$\alpha(x,y) \cong \frac{\partial W(x,y)}{\partial x} = (M + J_0)x + J_{45}y, \quad (8)$$

$$\beta(x,y) \cong \frac{\partial W(x,y)}{\partial y} = (M - J_0)y + J_{45}x, \quad (9)$$

If the principal meridians of the astigmatic WFE function are oriented horizontally and vertically (as in *Figure 4* for example), the coefficient $J_{45} = 0$. In that case, *Equation* 8 says wavefront vergence error in the horizontal plane is $M + J_0 = (\partial W/\partial x)/x$ and *Equation* 9 says the wavefront vergence error in the vertical plane is $M{-}J_0 = (\partial W/\partial y)/y$. These expressions are the three-dimensional expression of Prentice's rule (*Equation* 1) for wavefront vergence for the special case when the axis of astigmatism is 0° or 90°. However, the general case of arbitrary axis of astigmatism is complicated by the introduction of skew rays, as will be shown in the next section.

To determine the shape of the perimeter of the geometric PSF for the astigmatic example in *Figure 3* we use *Equation* 4 to map points from the margin of the circular pupil to the retinal plane. If the starting ray location is given in polar coordinates (R, θ) where R is pupil radius and θ is the meridian angle, then the Cartesian coordinates of the ray in the pupil plane are ($x = R\cos(\theta)$, $y = R\sin(\theta)$). Combining these expressions with *Equations* 4, 8, *and* 9 yields

$$\alpha = \frac{\partial W}{\partial x} = (M + J_0)x = (M + J_0)R\cos(\theta) = A\cos(\theta), \tag{10}$$

$$\beta = \frac{\partial W}{\partial y} = (M - J_0)y = (M - J_0)R\sin(\theta) = B\sin(\theta). \tag{11}$$

This pair of equations is recognised as the parametric form of an ellipse with semi-diameters A and B expressed as visual angles. (Although not considered here, the blur disk remains elliptical when the pupil in an astigmatic system is elliptical.[15]) As a numerical example, let the pupil radius R = 3 mm, power vector component M for defocus = 1 D, and the component J_0 for astigmatism = 2 D. Evaluating *Equations* 8 *and* 9 gives the major radius $A = (1 + 2)D*3$ mm = 9 mrad and the minor radius $B = (1 - 2)D*3$ mm = −3 mrad. The negative sign for β indicates the ray has crossed over to the opposite side of the optical axis, as shown in *Figure 3*.

As noted earlier, the irradiance of the geometric PSF depends on the area of the blur disk. The area of an ellipse with major and minor semi-diameters A and B is πAB. According to *Equations* 8 *and* 9, A and B are proportional to the vergence errors in the principal meridians. Although rotation of the axis of astigmatism will alter the power vector values associated with a wavefront, rotation has no effect on the principal vergence errors and therefore will have no effect on the area the blur ellipse. Thus we may conclude that the area of the geometric PSF is proportional to the product of vergence errors in the principal meridians. As noted earlier, wavefront vergence and curvature are equivalent for parabolic wavefronts in the paraxial domain, so the area of the elliptical PSF is also proportional to the product of principal curvatures of the wavefront aberration function.

In the field of mathematics, the product of principal curvatures of a surface is called the Gaussian curvature. Using this language, we conclude that the area of the blur ellipse caused by sphero-cylindrical refractive error is proportional to the Gaussian curvature of the wavefront aberration function. Thus the irradiance of the blur ellipse is inversely proportional to the Gaussian curvature of the WFE function. In the next section we show that this basic result can be applied to eyes with higher-order aberrations by approximating each local region of the WFE function as a sphero-cylindrical surface with Gaussian curvature that varies with position across the exit pupil.

Vergence error matrix and the geometric PSF

Equations 8 *and* 9 derived above are mapping functions that provide the visual coordinates (α, β) of light on the retina arising from some point (x,y) in the exit pupil. If we envision light propagation by individual rays carrying energy from the pupil plane to form spots of light in the retinal plane, then the distribution of those spots according to *Equations* 8 *and* 9 is a first approximation to the geometrical PSF. In the field of optical engineering, this distribution of light spots is called a 'spot diagram' and is used to determine where the image will be bright (region of high spot density) or dim (region of low spot density). Below we show how a refined approximation to the PSF may be obtained by assigning a value to each spot that represents the local retinal irradiance inferred from the Gaussian curvature of the WFE surface at the point of origin of the ray that produced the spot. High WFE curvature (positive or negative) indicates more blurring, so retinal irradiance is low. Conversely, low WFE curvature (positive or negative) indicates less blurring, so retinal irradiance is high. Thus to proceed we need a general way to compute the principal curvatures of the WFE surface at any (x,y) location for any orientation of the local principal meridians. The method of choice, described next, is based on the vergence error matrix derived from a second-order Zernike approximation to the local WFE surface.

The previous section included an example of astigmatic wavefronts with principal meridians oriented horizontally and vertically, in which case horizontal slope depends only on pupil coordinate x and vertical slope depends only on y. More generally, when the astigmatic axis is oriented obliquely the horizontal and vertical components of WFE slope at the pupil location (x,y) both depend on both x and y coordinates of the point of interest according to *Equations* 8 *and* 9. In the analogous context of describing the refraction of rays of light by sphero-cylindrical lenses with arbitrary axis, Long used Prentice's rule to formulate the problem and its solution mathematically by constructing a dioptric power matrix.[16] Later, Keating[4,7] and Harris[5,8] built on Long's foundation to develop dioptric power matrices useful for tracing rays and wavefronts through thick astigmatic systems. Although optical power and wavefront vergence are distinctly different entities, they are intimately related because lenses have the power to change the vergence of light. Consequently, refraction of an incident plane wave by a thin lens (or single refracting surface) produces a wavefront with reduced vergence matrix equal to the dioptric power matrix of the lens. Although thick astigmatic systems may require an asymmetric dioptric power matrix to describe the transference of rays, the emerging wavefront can be still be described by a symmetric vergence error matrix equal to the back-vertex dioptric power matrix of the thick system.[7] When written in power vector notation, this vergence error matrix V is[6]

$$V = \begin{bmatrix} M + J_0 & J_{45} \\ J_{45} & M - J_0 \end{bmatrix}. \tag{12}$$

For ordinary sphero-cylindrical refractive errors, the matrix element $M + J_0$ is the vergence of the WFE in the horizontal meridian of the pupil and the element $M - J_0$ is the WFE vergence in the vertical meridian of the pupil. When the axis of the astigmatism is obliquely oriented (i.e. is neither vertical nor horizontal), a skew component of wavefront vergence also exists for points on the x- and y-axes. The matrix element J_{45} represents this skew component of vergence.

The vergence error matrix plays a key role in determining the geometric PSF because, as Keating (1980) showed, the determinant of a dioptric power matrix equals the product of principal powers of a lens regardless of lens orientation relative to the x, y coordinate systems. This is true also for the vergence error matrix V, which has a determinant

$$|V| = M^2 - \left(J_0^2 + J_{45}^2\right), \tag{13}$$

$$|V| = M^2 - J^2 = (M + J)(M - J), \tag{13a}$$

Converting from rectangular (*Equation* 13) to polar (*Equation* 13a) forms of the power vector notation is based on the Pythagorean relationship $J^2 = J_0^2 + J_{45}^2$, which confirms that the determinant $|V|$ equals the product of principal vergence errors.

In summary, the determinant of the vergence error matrix V equals the product of principal vergence errors, i.e. the Gaussian curvature of the WFE surface. Thus, in the absence of higher-order aberrations, the area of the blur ellipse is proportional to $|V|$, and irradiance is inversely proportional to $|V|$, regardless of the orientation of the astigmatic axis.

When higher-order aberrations are present, we envision subdividing the WFE surface into a mosaic of small, circular areas (or tiles) of uniform spacing and diameter rather like the action of a Hartmann screen used in wavefront aberrometers.[17] At the centre of each tile lies a ray indicating the direction of propagation of light in that local area towards the image plane according to the mapping *Equations* 8 *and* 9. The local shape of the WFE surface for a tile centred on the point (x,y) is approximated by a sphero-cylindrical wavefront with vergence error matrix $V(x,y)$ that produces a local blur ellipse with area proportional to the local Gaussian curvature $G(x,y) = |V(x,y)|$ and irradiance inversely proportional to $G(x,y)$. In this way a sampled WFE surface represented by a uniformly-spaced mosaic of circular tiles in the exit pupil, each characterised by the local Gaussian curvature $G(x,y)$, yields a sampled retinal image comprised of non-uniformly spaced blur ellipses, each of which has an irradiance that is inversely proportional to $G(x,y)$. Assigning this irradiance value to the corresponding ray yields the geometric PSF as an enhanced spot diagram for which each spot represents the position and local irradiance in the image produced by light from the corresponding part of the pupil.

In principle, the area of each tile in the WFE surface can shrink to infinitesimal size while the number of tiles and rays grows infinitely large. In the limit, as tile size goes to zero, the result is a spatially continuous retinal image formed by the propagation of a spatially continuous wavefront. Light distribution in this continuous PSF may be determined analytically using *Equation* 13a if the matrix elements are written as continuous functions of pupil coordinates (x,y). Optically we envision the aberrated wavefront becoming distorted transversely as it propagates because local regions are steeper or flatter than the reference sphere, which is why the wavefront will not converge to a perfect point image. This transverse distortion is perpendicular to the direction of light propagation and therefore affects the irradiance (light flux/unit area) produced by each infinitesimal, blurred contribution to the retinal image. To envision this phenomenon, imagine a rubber sheet that thins when stretched and thickens when compressed. If thin regions represent low flux density (i.e. irradiance) and thick regions representing high flux density, then the distribution of thickness in the rubber sheet is analogous to the geometric PSF formed by a wavefront distorted by propagation from pupil to retina.

Practical application of the method described above requires knowledge of the local vergence error matrix V at a multitude of sample points in the exit pupil. If we write the vergence error matrix generically as

$$V(x,y) = \begin{bmatrix} A & B \\ C & D \end{bmatrix}, \tag{14}$$

then the elements A, B, C, D are all functions of (x,y) and each may be determined three ways, depending on how the wavefront aberrations are specified:

$$A = \frac{\partial\alpha}{\partial x} = \frac{\partial^2 W}{\partial x^2} = M + J_0$$
$$= \text{horizontal rate of change in horizontal slope},$$

$$B = \frac{\partial\beta}{\partial x} = \frac{\partial^2 W}{\partial x \partial y} = J_{45}$$
$$= \text{horizontal rate of change in vertical slope},$$

$$C = \frac{\partial\alpha}{\partial y} = \frac{\partial^2 W}{\partial y \partial x} = J_{45}$$
$$= \text{vertical rate of change in horizontal slope},$$

$$D = \frac{\partial\beta}{\partial y} = \frac{\partial^2 W}{\partial y^2} = M - J_0$$
$$= \text{vertical rate of change in vertical slope}.$$

The top row $[A\ B]$ of matrix V is thus the gradient of horizontal slopes, $\nabla(\partial W/\partial x)$, and the bottom row $[C\ D]$ of V is the gradient of vertical slopes, $\nabla(\partial W/\partial y)$.

For numerical calculations using a finite number of rays sampling the WFE surface, each of the quantities A, B, C, D needs to be specified at every (x,y) location in the grid of pupil locations. These numerical values may be conveniently stored in a matrix the same size as the matrix of pupil sample locations. The PSF irradiance at the retinal point (α, β) corresponding to ray location (x,y) is proportional to $1/|V| = 1/(AD-BC)$. Evaluating the determinate explicitly as the scalar product (e.g. A.*D − B.*C in MATLAB (www.mathworks.com)) efficiently computes the Gaussian curvature of WFE for all sample points in a single operation. Mapping the inverse of these Gaussian curvature values onto the spot diagram determined by the mapping *Equations* 8 *and* 9 thus yields the geometric PSF. The only caveat is that, in general, a uniformly-spaced grid of sample points in the pupil plane produces non-uniformly spaced spots in the spot diagram. If a uniform image grid is needed for subsequent use, then interpolation or a weighted histogram are two possible solutions.

The foregoing development assumed the distribution of light in the pupil plane is uniform but in general the exit pupil irradiance should be scaled by the eye's transmission function $T(x,y)$. For example, a cataract may attenuate light non-uniformly across the pupil, or the Stiles-Crawford effect may attenuate the visual intensity of light more near the pupil margins. Thus the general expression for the geometric PSF is

$$I(\alpha,\beta) = \frac{T(x,y)}{|V(x,y)|} = \frac{T(x,y)}{A(x,y)D(x,y) - B(x,y)C(x,y)} = \frac{T(x,y)}{G(x,y)}, \tag{15}$$

where the implicit image coordinates $(\alpha(x,y), \beta(x,y))$ are computed from the gradient of the wavefront aberration function as indicated by the mapping *Equations* 8 *and* 9.

As indicated by *Equation* 14, there are four options for computing the elements A, B, C, D used to populate the vergence matrix V so that its determinate can be calculated for mapping irradiance onto the spot diagram. This report has emphasised the use of dioptric power vector components (M, J_0, J_{45}) of the wavefront error because of their familiarity in the field of optometric and visual optics. In practice, however, it may be more convenient to populate the matrix V with the gradients of the mapping functions in *Equations* 8 *and* 9. The result is known as the Jacobian matrix[18]

$$J = \begin{bmatrix} \nabla\left(\frac{\partial W}{\partial x}\right) \\ \nabla\left(\frac{\partial W}{\partial y}\right) \end{bmatrix} = \begin{bmatrix} \frac{\partial\alpha}{\partial x} & \frac{\partial\alpha}{\partial y} \\ \frac{\partial\beta}{\partial x} & \frac{\partial\beta}{\partial y} \end{bmatrix}. \tag{16}$$

In our optical application, the determinant of the Jacobian matrix quantifies how the area of a local region in the pupil plane changes when rays of light map the region to the image plane.[19] It is this change in area that is responsible for non-uniform distribution of light in the geometrical PSF even when the distribution of light in the pupil plane is uniform. Mahajan used the Jacobean matrix in his textbook *Equations* 4–10 for the geometric PSF.[20]

Rather than using the ray mapping equations, we can compute the gradients of horizontal and vertical slopes in *Equation* 16 directly from the wavefront error function to obtain a matrix of second derivatives, which is recognized as a Hessian matrix

$$H(x,y) = \begin{bmatrix} \frac{\partial^2 W}{\partial x^2} & \frac{\partial W}{\partial x \partial y} \\ \frac{\partial W}{\partial x \partial y} & \frac{\partial^2 W}{\partial y^2} \end{bmatrix}. \tag{17}$$

Hessian matrices are commonly used in image processing, computer vision, and other applications[21] and in Mahajan's textbook *Equations* 4–11 for the geometrical PSF.[20] The determinant of the Hessian matrix H can be taken as a definition of Gaussian curvature, which we have interpreted optically as the area of the blur ellipse attributed to a local patch of wavefront when that patch is approximated by a sphero-cylindrical surface.

In summary, the Jacobian matrix J formulated from the gradients of WFE slopes in *Equation* 16 and the Hessian matrix H formulated from WFE curvature in *Equation* 17 are both equal to the vergence error matrix V formulated from ray vergence in *Equation* 14. The determinants of all three of these matrices are equal to the Gaussian curvature of the WFE function and therefore the PSF can be written in terms of each of them,

$$I(\alpha,\beta) = \frac{T(x,y)}{G(x,y)} = \frac{T(x,y)}{|V(x,y)|} = \frac{T(x,y)}{|J(x,y)|} = \frac{T(x,y)}{|H(x,y)|}. \tag{18}$$

Caustics in the geometric PSF

Caustics are image features with very high irradiance.[22,23] The simplest example of a caustic is the geometric point image created by a perfect optical system. The next simplest example is the line image formed by an astigmatic system for which the image plane is located at one extreme of the interval of Sturm. According to the geometrical optical theory outlined above, such caustics form when the area of a local blur ellipse in the image plane approaches zero. Local irradiance in the image is inversely proportional to the ellipse area, which we have shown is proportional to the product of principal curvatures of the WFE, i.e. the Gaussian curvature of the wavefront aberration function. When Gaussian curvature goes to zero at some location on the wavefront, its inverse (image irradiance) grows infinitely large at the image location where the associated ray intersects the image plane. Zero Gaussian curvature in the WFE function will occur when one of the principal curvatures is zero, in which case the WFE surface is locally cylindrical with zero curvature in a direction parallel to the cylinder's axis. An example is shown in *Figure 5a* for the simplest possible case of globally cylindrical WFE without higher-order aberrations. In clinical notation, this example is for an eye with refractive error 0 D sphere, −4 D cylinder, axis 22.5° counter-clockwise from the horizontal. The short white lines overlaid on the WFE map indicate the local axis of the WFE at multiple sample points. Since there are no higher-order aberrations in this example, every patch of wavefront has the same axis as every other patch, so all of the axes are oriented 22.5° to the horizontal.

Since the spherical component of refractive error is zero in this example, one of the local principal curvatures is zero at every sample point, so the Gaussian curvature is zero everywhere on the WFE surface. Thus the entire wavefront will contribute to the formation of caustics in the retinal image plane. We may envision the formation of that caustic by considering a small patch of wavefront that propagates to the image plane along a direction associated with the associated ray. No spreading of light will occur in a direction parallel to the local astigmatism axis because there is zero wavefront curvature along that axis. Since all the axes are parallel in this example, no part of the wavefront will produce spreading of light in the 22.5° direction. To the contrary, wavefront curvature is maximum in the orthogonal direction of 112.5° so all parts of the WFE function will produce blurring in that direction. Thus we should expect the retinal image to be a narrow focal line inclined at 112.5° (the direction of maximum blurring), which is confirmed by the computed geometric PSF as shown in *Figure 5b*.

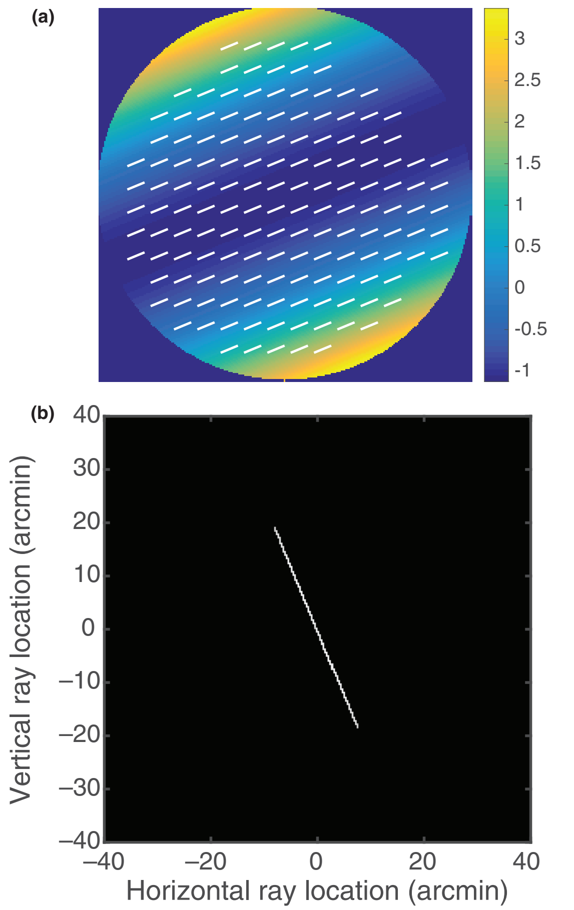

Figure 5. Wavefront error (panel a, top) and geometric optical point-spread function (PSF) (panel b, bottom) for an astigmatic system with line focus in the image plane. In order to render the PSF for publication, logarithmic compression of the irradiance scale is used to display the four orders of magnitude range in this example. Zernike aberration coefficients are C2-2 = - 0.65, C20 = 0.65, C2+2 = - 0.65, pupil diameter = 3 mm.

Applying this patch-wise model of image formation to imaging systems with higher-order aberrations leads to the conclusion that any portion of the WFE surface for which Gaussian curvature = 0 will contribute to the formation of caustics in the image. An example of radiating 'starburst' caustics produced in a system with coma and spherical aberration in addition to sphero-cylindrical refractive error is shown in *Figure 6*. Maps of the two principal curvatures over the domain of a circular pupil are shown in the top

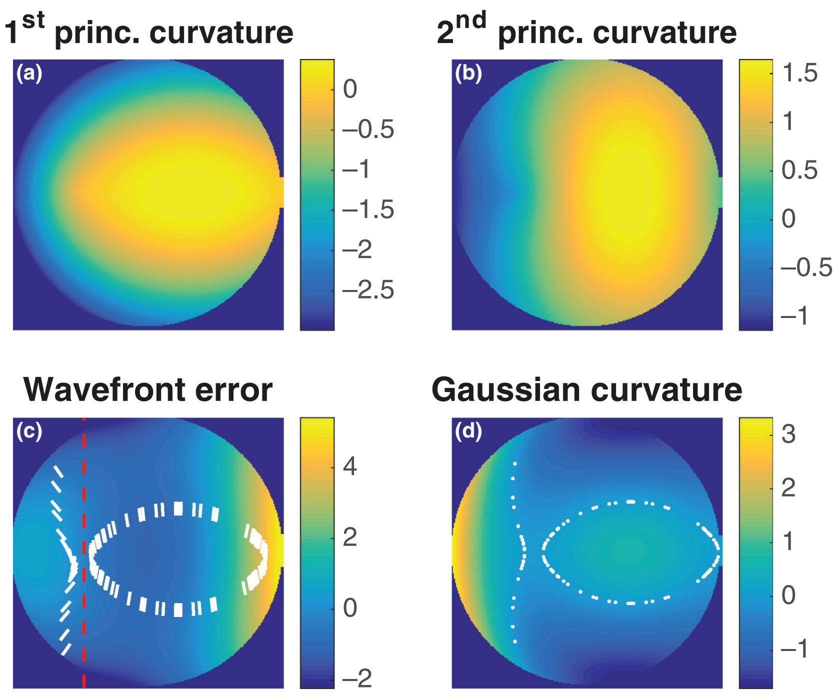

Figure 6. Wavefront error (c), principle curvatures (a,b), and Gaussian curvature (d) maps for an optical system with Zernike spherical aberration ($C_4^0 = -0.15\mu$), vertical coma ($C_3^1 = 0.3\mu$), astigmatism ($C_2^2 = 1\mu$), and defocus ($C_2^0 = 0.5\mu$). Pupil diameter = 6 mm.

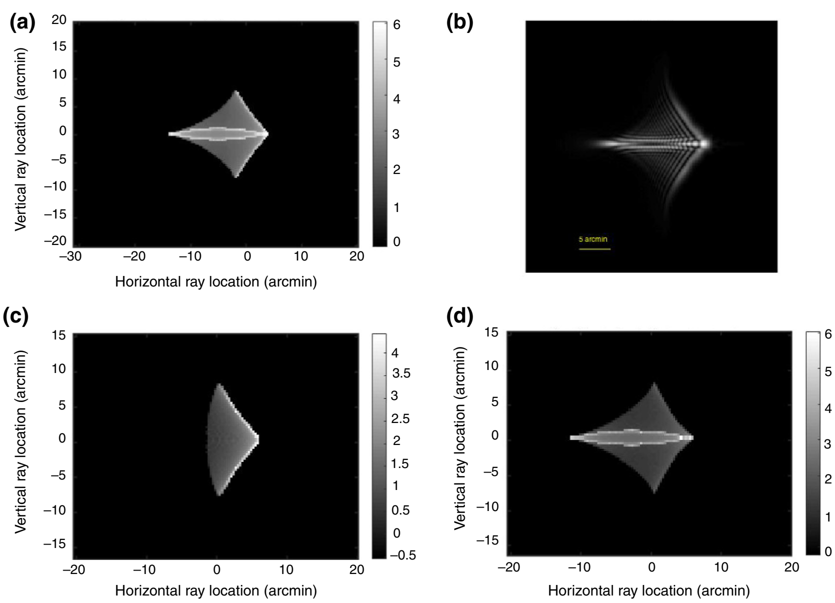

Figure 7. (a) Geometric PSF for system in *Figure 6*. (b) Physical optics optical point-spread function (PSF) for the same system. Both PSFs are shown on the same spatial scale but different intensity scales to improve the display of the geometric PSF. (c) Geometric PSF obtained when light transmission is blocked for the right-hand side of the dashed line in *Figure 6c*. (d) Geometric PSF obtained when light transmission is blocked for the left-hand side of the dashed line in *Figure 6c*. Panels a, c, d use logarithmic compression of computed irradiance values. Maximum and minimum PSF values assigned to the maximum and minimum pixel luminances in those panels were adjusted to render details of interest.

row of panels and their product, the Gaussian curvature, is shown in the bottom right panel. A sample of critical locations for which Gaussian curvature = 0 are indicated by white dots. In this example, the dots separate naturally into two groups, an oval of dots on the right side of the pupil and a vertical string of dots on the left. The local axis of astigmatism associated with each of these critical locations is displayed in the lower left panel, on a backdrop of the wavefront error function. This lower left panel shows that all of the axes associated with the oval locus of critical points are oriented vertically, so they will contribute to horizontally oriented caustics. To the contrary, the axes associated with the vertical string of critical points are tilted at approximately ±45° to the horizontal, so they will contribute to obliquely oriented caustics.

As predicted, the geometric PSF computed from the inverse of the Gaussian curvature map contains caustics that are oriented horizontally and obliquely as shown in *Figure 7a*. The range of PSF irradiance values spans six orders of magnitude in this example but, in reality, diffraction effects will keep irradiance finite as may be seen in the physical optics PSF displayed in *Figure 7b*. To verify the mapping of critical points in the pupil plane to caustics in the image plane, the transmission factor $T(x,y)$ in *Equation* 18 was set to zero on one side or the other of the dashed line in *Figure 6c*. Transmitting just the left side of the pupil blocks the horizontal caustics, leaving just the obliquely oriented caustics in *Figure 7c*. Similarly, transmitting just the right side of the pupil blocks the oblique caustics, leaving just the horizontal caustics in *Figure 7d*.

Discussion: practical implementation

Ophthalmic wavefront aberrometers that measure wavefront slopes in the horizontal and vertical direction (e.g. the Hartmann-Shack method[17]) provide the raw data needed to rapidly compute the geometric PSF from the Jacobian matrix. However, the discrete PSF will have the same number of samples as the raw measurements, which may be inadequate for some applications. In that case, derivatives of Zernike polynomials fit to the slope measurements may be used to interpolate the slope data, thereby increasing the size of the Jacobian matrix and the density of points in the geometric PSF at the cost of increased computational time.

For theoretical work, it may be more convenient to express the WFE function by its Zernike expansion as a weighted sum of polynomials, for which the Jacobian matrix may be computed using symbolic mathematical software [e.g. Mathematica (www.wolfram.com), Maple (www.maplesoft.com), or MATLAB symbolic toolbox (www.mathworks.com)]. For complex optical systems with many elements, a more comprehensive computational method may be preferred.[24]

Acknowledgements

I am indebted to E. Sarver and J. Rubinstein for valuable discussions regarding the relationship between the Hessian matrix, the Jacobian matrix, and Gaussian curvature.

Disclosure

The author reports no conflicts of interest and has no proprietary interest in any of the materials mentioned in this article.

References

1. Thibos LN, Hong X, Bradley A & Applegate RA. Accuracy and precision of objective refraction from wavefront aberrations. *J Vis* 2004; 4: 329–351.
2. Thibos LN. Formation and sampling of the retinal image. In: *Seeing (Handbook of Perception and Cognition)*, (De Valois K, ed.). Academic Press: London, 2000; pp. 1–54.
3. Prentice CF. *Optical Lenses, Dioptric Formulae for Combined Cylindrical Lenses: The Prism-Dioptry, and Other Optical Papers*. Keystone: Philadelphia, PA, 1907.
4. Keating MP. Dioptric power in an off-axis meridian: the torsional component. *Am J Optom Physiol Opt* 1986; 63: 830–838.
5. Harris WF. Wavefronts and their propagation in astigmatic optical systems. *Optom Vis Sci* 1996; 73: 606–612.
6. Thibos LN, Wheeler W & Horner DG. Power vectors: an application of Fourier analysis to the description and statistical analysis of refractive error. *Optom Vis Sci* 1997; 74: 367–375.
7. Keating MP. A system matrix for astigmatic optical systems: I. Introduction and dioptric power relations. *Am J Optom Physiol Opt* 1981; 58: 810–819.
8. Harris WF. Dioptric power: its nature and its representation in three- and four-dimensional space. *Optom Vis Sci* 1997; 74: 349–366.
9. Xu R, Kollbaum P, Thibos L, Lopez-Gil N & Bradley A. Reducing starbursts in highly aberrated eyes with pupil miosis. *Ophthalmic Physiol Opt* 2018; 38: 26–36.
10. Xu R, Thibos L, Lopez-Gil N, Kollbaum P & Bradley A. Psychophysical study of the optical origin of starbursts. *J Opt Soc Am A Opt Image Sci Vis* 2019; 36: B97–B102.
11. Smith G. Angular diameter of defocus blur discs. *Am J Optom Physiol Opt* 1982; 59: 885–889.
12. Rosello S, Thibos L & Mico V. Step-along power vector method for astigmatic wavefront propagation. *Ophthalmic Physiol Opt* 2014; 34: 295–308.
13. Raasch TW. Propagation of aberrated wavefronts using a ray transfer matrix. *J Opt Soc Am A Opt Image Sci Vis* 2014; 31: 964–967.

14. ANSI (American National Standards Institute). *American national standard Z80.28 for ophthalmics - methods for reporting optical aberrations of eyes*. 2010.
15. Harris WF. Aperture referral in heterocentric astigmatic systems. *Ophthalmic Physiol Opt* 2011; 31: 603–614.
16. Long WF. A matrix formalism for decentration problems. *Am J Optom Physiol Opt* 1976; 53: 27–33.
17. Thibos LN. Principles of Hartmann-Shack aberrometry. *J Refract Surg* 2000; 16: S563–S565.
18. Buck RC. *Advanced Calculus*. Waveland Press, Inc.: Long Grove, IL, 1978.
19. Wikipedia. *Jacobian matrix*. Available from: https://en.wikipedia.org/wiki/Jacobian_matrix_and_determinant (Accessed May 2019).
20. Mahajan VN. *Optical Imaging and Aberrations*. SPIE Optical Engineering Press: Bellingham, Washington, 1998.
21. Wikipedia. *Hessian matrix*. Available from: https://en.wikipedia.org/wiki/Hessian_matrix (Accessed May 2019).
22. Kravtsov YA & Orlov YI. *Caustics, Catastrophes and Wave Fields*, 2nd edn. Springer: New York, NY, 1999.
23. Nye JF. *Natural Focusing and Fine Structure of Light*. Institute of Physics Publishing: Bristol, UK, 1999; p. 328.
24. Liu CS & Lin PD. Computational method for deriving the geometric point spread function of an optical system. *Appl Opt* 2010; 49: 126–136.
25. Tscherning M. *Physiologic Optics*. The Keystone Press: Philadelphia, PA, 1904.
26. Howland HC & Howland B. A subjective method for the measurement of monochromatic aberrations of the eye. *J Opt Soc Am* 1977; 67: 1508–1518.
27. Rubinstein J. On the geometry of visual starbursts. *J Opt Soc Am A Opt Image Sci Vis* 2019; 36: B58–B64.

Appendix

Envisioning the formation of the geometric optical point-spread function (PSF) is aided by dynamic simulation of propagating wavefronts of light using geometrical optics. Four simulations provided as Supporting Information (Videos S1–S4) are described briefly below. The computer simulations were created by the same custom MATLAB programs used to produce *Figures 5–7* in the Results section. Each simulation has two panels: the left panel shows the wavefront and the right panel shows the corresponding irradiance of the beam of light. Wavefront propagation is visualised by observing changes in the grid of equally spaced horizontal and vertical lines imprinted on the wavefront as it passes through the exit pupil. The outer margin of the blur patch shows how the beam changes shape as the wavefront propagates. The dynamic simulations begin after the wavefront has propagated two-thirds of the distance to the focal point.

Simulation 1: an optically perfect myopic eye

Computer simulation of wavefront propagation through an optically perfect eye with $M = -1$D of myopia (6 mm pupil diameter) is displayed in supplementary movie *waveMovie_M = −1D.avi*. *Appendix Figure 1* shows the first frame of the movie, which depicts the wavefront after propagating the first two-thirds of the distance to the focal point. Without aberrations the grid of horizontal and vertical lines attached to the wavefront remains uniformly spaced at all propagation distances and therefore the circular beam has uniform irradiance. As the wavefront propagates towards the focal point, the spacing between grid lines is reduced, and therefore the spatial density of light flux increases. After passing through the focal point (a point-caustic), the diverging beam produces a uniformly illuminated blur circle on the retina. This simulation demonstrates the principle of Tscherning's subjective aberroscope[25] constructed from a wire mesh near the eye that casts a grid of shadows on the wavefront, plus a defocusing lens to enlarge the retinal blur patch sufficiently for the observer to report any distortions of the grid produced by optical aberrations.

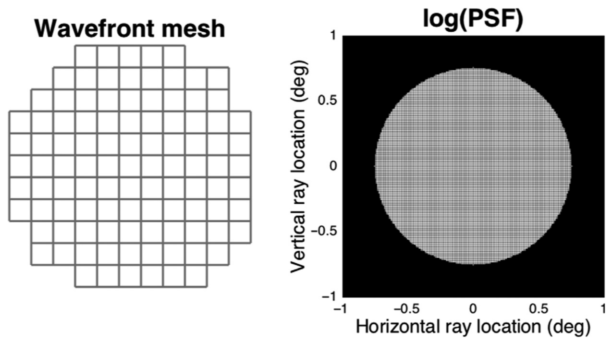

Simulation 2: an astigmatic eye (with-the-rule)

Computer simulation of wavefront propagation through a well-focused eye ($M = 0$, 6 mm pupil diameter) with $J_0 = 1$ D of with-the-rule astigmatism (axis 180°) is displayed in supplementary movie *waveMovie_J0 = 1D.avi*. Because the grid lines are parallel to the astigmatic principal meridians, the grid lines remain vertical and horizontal as shown in *Appendix Figure 2*. However, the horizontal lines are more closely spaced than the vertical lines after propagation because the eye's refractive power is greater in the vertical meridian in this eye. Nevertheless, all rectangular tiles in the wavefront mesh have the same area, so the elliptical beam has uniform irradiance. As the wavefront propagates, all grid tiles collapse to zero area simultaneously, resulting in a focal line (a line-caustic). After passing through the line focus, the diverging light produces an elliptical beam that evolves into a circular patch of wavefront with uniform irradiance on the retina.

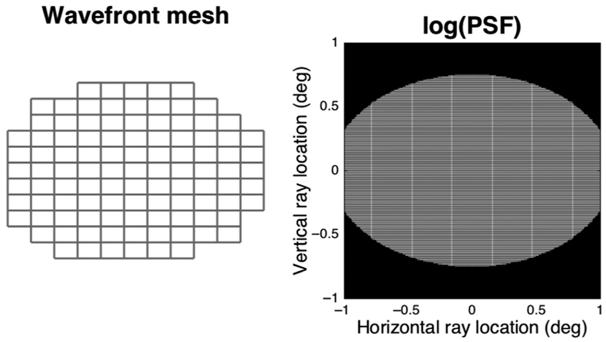

Simulation 3: an astigmatic eye (oblique axis)

Computer simulation of wavefront propagation through a well-focused eye ($M = 0$, 6 mm pupil diameter) with $J_{45} = 1$ D of oblique astigmatism (axis 45°, to visualise skew rays) is displayed in supplementary movie *waveMovie_J45 = +1D.avi*. *Appendix Figure 3* shows the wavefront after propagating the first two-thirds of the distance to the focal point. Counter-rotation of the grid lines produces a scissors-like action that distorts the wavefront and produces a 90° rotation of the grid in the retinal plane. This simulation demonstrates the principle of Howlands' crossed-cylinder aberroscope[26] constructed from a wire mesh plus a Jackson cross-cylinder lens to produce a circular blur patch that allowed observers to report any distortions of the grid produced by optical aberrations.

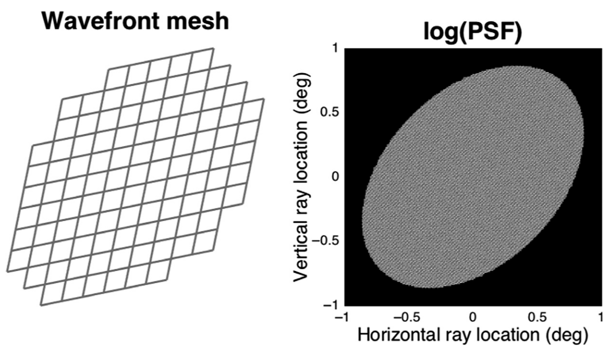

Simulation 4: an eye with spherical aberration (Z_4^0) and fourth order astigmatism (Z_4^{-2})

Computer simulation of wavefront propagation through an eye with fourth order aberrations is displayed in supplementary movie *waveMovie_HOA.avi*. Zernike coefficients (in microns) for the wavefront error were $C_4^0 = 0.0745$; $C_4^{-2} = 0.3162$; $C_2^0 = 0.2887$ $C_2^{-2} = 1.2247$ (6 mm pupil diameter). *Appendix Figure 4* shows non-uniform wavefront distortion that produces a curved caustic at the beam margin that evolves into line caustics in the retinal plane. This simulation demonstrates a recently proven optical theorem stating that a mixture of higher-order aberrations of the same order always produces radial line caustics in the focal plane.[27]

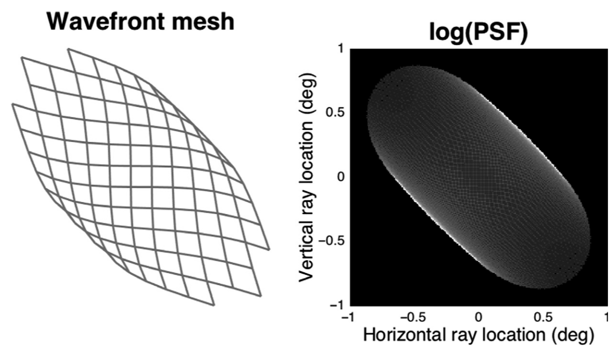

Supporting Information

Additional Supporting Information may be found in the online version of this article:

Video S1. Supplementary movie *waveMovie_M=-1D.avi*.

Video S2. Supplementary movie *waveMovie_J0=+1D.avi*

Video S3. Supplementary movie *waveMovie_J45=+1-D.avi*.

Video S4. Supplementary movie *waveMovie_HOA.avi*.